

Article

Improvement of Simple Test Cell Design for Cathode Microstructure Study in Tubular-Type Sodium–Metal Chloride Batteries

Byeong-Min Ahn ^{1,2} , Cheol-Woo Ahn ^{1,*}, Byung-Dong Hahn ¹, Jong-Jin Choi ¹, Yang-Do Kim ² , Sung-Ki Lim ³ and Joon-Hwan Choi ^{1,*}

¹ Korea Institute of Materials Science (KIMS), Changwon 51508, Korea

² Department of Materials Science and engineering, Pusan National University, Busan 46241, Korea

³ Department of Material Chemistry and Engineering, Konkuk University, Seoul 143-701, Korea

* Correspondence: cheoruanh@kims.re.kr (C.-W.A.); jchoi@kims.re.kr (J.-H.C.); Tel.: +82-55-280-3406 (C.-W.A.)

Abstract: Sodium–metal chloride batteries are suitable alternatives in battery energy storage systems (BESSs), since they are widely known as a type of high-safety battery. To accurately analyze the cathode microstructure of sodium–metal chloride batteries, in this study, we demonstrate the improved tubular-type simple test cell. This improved tubular-type simple test cell was supplemented from the setbacks of our previous test cell, such as a leak, Ni current collector wavering, and sodium wicking. Through testing of the improved test cells, we focus on cathode microstructure analysis, owing to the elimination of the external failure factors mentioned above. The group of improved test cells have a lower capacity gap of 9.5% in the 1st cycle than the capacity gap of previous test cells (37.2%). This result indicates the advancement of reproducibility. Moreover, the improved test cell has a long life of approximately 7200 h by changing the previous test cell structure. In particular, it is expected that this improved tubular simple test cell can advance the research of tubular-type sodium–metal chloride batteries in a small and academic laboratory.

Keywords: energy storage systems; sodium–nickel chloride batteries; tubular-type cell; simple test cell



Citation: Ahn, B.-M.; Ahn, C.-W.; Hahn, B.-D.; Choi, J.-J.; Kim, Y.-D.; Lim, S.-K.; Choi, J.-H. Improvement of Simple Test Cell Design for Cathode Microstructure Study in Tubular-Type Sodium–Metal Chloride Batteries. *Batteries* **2022**, *8*, 163. <https://doi.org/10.3390/batteries8100163>

Academic Editors: Quanqing Yu, Yonggang Liu and Xiaopeng Tang

Received: 20 July 2022

Accepted: 3 October 2022

Published: 7 October 2022

Publisher's Note: MDPI stays neutral with regard to jurisdictional claims in published maps and institutional affiliations.



Copyright: © 2022 by the authors. Licensee MDPI, Basel, Switzerland. This article is an open access article distributed under the terms and conditions of the Creative Commons Attribution (CC BY) license (<https://creativecommons.org/licenses/by/4.0/>).

1. Introduction

Secondary batteries are widely used in various forms, ranging from mobile devices to electric cars and energy storage systems (ESSs). The increased usage of batteries provides convenience in modern society, but the risk of battery explosion is also increased. In particular, the explosion of a large ESS-scale battery is entirely different from that of a small-sized battery. One of the prevention methods of battery explosion is the safety design in a battery system that is actively studied presently [1–3]. However, in addition to safety design, the selection of a safe battery, such as a sodium–metal chloride battery (Na/MCl₂ battery), is another excellent prevention method against battery explosion [4,5]. The Na/MCl₂ battery has high energy efficiency, no sensitivity to the external environment because it is operated at a high temperature of approximately 300 °C, and a perfectly sealed cell structure. Furthermore, the crack recovery mechanism on the ceramic separator surface in a Na/MCl₂ battery is an exceptional advantage for safety, dissimilar to other secondary batteries [6]. Despite these advantages, Na/MCl₂ battery research is difficult in a small and academic laboratory. In the cathode and anode, metal (Ni, Fe, among others), NaCl, NaAlCl₄, and Na are included, and all of these are highly sensitive in the general atmosphere. Consequently, many types of exclusive equipment are necessary to assemble a hermetically sealed cell.

To easily and accurately verify cathode microstructure behavior in the tube-type cell, a simple test cell must be designed. Similar studies, such as planar-type simple test cell,

were published, however, a simple test cell design for tubular-type Na/MCl₂ battery was not reported until now. In recent studies on tube-type cells, commercial Na/MCl₂ batteries were used instead of the test cells [7–12]. Contrastingly, a planar-type test cell was recently published and actively applied in research [13–22]. However, a design of the cathode microstructure of the planar-type cell is difficult to apply to a tube-type cell. Therefore, a tube-type simple test cell has to be designed and developed to activate a tubular Na/MCl₂ battery test in small and academic laboratory research.

2. Materials and Methods

2.1. Preparation of Cathode Materials

The cathode granule used in a Na/NiCl₂ cell contained Ni (99.7%, 2.5 µm, standard grade, Vale, Singapore) and NaCl (98%, Sigma Aldrich, Burlington, MA, USA) powders. Ni and NaCl powders were mixed with low-energy ball milling without balls for 2 h. After mixing, the Ni–NaCl granules were made by a roller compactor (Seong-jin machine Co., Gyeonggi-do, Korea). Moreover, in the cathode, the 2nd electrolyte (NaAlCl₄) and sulfur (reagent grade, —100-mech, Sigma Aldrich, Burlington, MA, USA) were added, and the sulfur was used to remove an oxidation layer on the surface of the metal particles [23]. The 2nd electrolyte was synthesized using NaCl and AlCl₃ (99.985%, Alfa Aesar, Ward Hill, MA, USA) powders at 300 °C for 1 h. In the Na/(Ni, Fe)Cl₂ cell, Ni and Fe (99.5%, 6.5 µm, BASF, Ludwigshafen, Germany) powders were mixed with a Turbula-type T2C shaker mixer (Willy A. Bachofen AG, Uster, Switzerland) for 2 h to reinforce the connection between the metal particles. Except for the Ni–Fe mixing process, all other preparation steps are same as that of the Na/NiCl₂ cell. The cathode materials were verified using a scanning electron microscope (SEM, IT-300; JEOL Co., Tokyo, Japan) and X-ray diffraction (XRD, D/Max-2500, Rigaku, Tokyo, Japan).

2.2. Design and Fabrication of the Tubular Type Simple Test Cell

Our simple test cell was developed continuously, and the design of the previous test cell was mentioned before in our studies [24,25]. Figure 1a shows the previous test cell structure that was used in our preceding research. Al foil and Ni foam were wrapped on the BASE surface. It is difficult to control the wrinkles on the BASE surface in Al foil wrapping since this process is performed by hand. These wrinkles could be the cause of sodium wicking that is one of the problems in previous test cell. Inclusive of sodium wicking, there were three specific problems in our previous test cell structure, with a leak and Ni current collector wavering. Therefore, in this research, we focused on a supplementation of previous test cell problems. As shown in Figures 1b and 2, the improved simple test cell consists of β"-alumina solid electrolyte (BASE; Ionotec, Berkeley, UK), Ni current collector, cell case, cathode, and Na metal in the anode. The outside surface of the BASE tube was coated with carbon paste (Research Institute of Industrial Science and Technology (RIST), Pohang-si, Korea) to improve the wettability of Na melt to the BASE surface [14]. The C-coated BASE tube was heat-treated at 230 °C for 30 min to remove a polymer and water contained in the carbon paste (Figure 1b). Ni current collector was settled in the BASE tube and the inside of the BASE, the tube was filled with cathode granules and NaAlCl₄. The bottom of the Ni current collector had stands for keeping the position in middle of the BASE tube. The melted sodium metal was filled in the Ni cell case before test learning. At the end of filling additional Na metal in the Ni case (anode), the prepared BASE tube was assembled in the Ni case. In our simple test cell, a Teflon cap and a hose clamp were applied for closing the package instead of the hermetic seal in commercial cells. The Teflon cap naturally closes the opening space due to expansion at an operation temperature of 300 °C. Moreover, Teflon is chemically stable on NaAlCl₄.

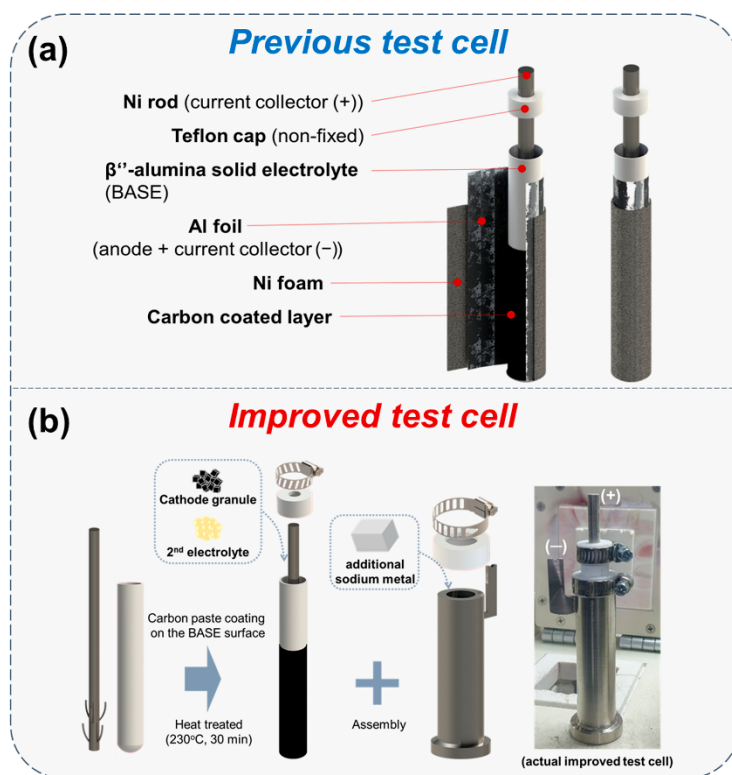


Figure 1. Schematic diagram of previous test cell and improved test cell. (a) Structure of previous test cell; (b) cell assembly process and photo of the actual improved test cell.

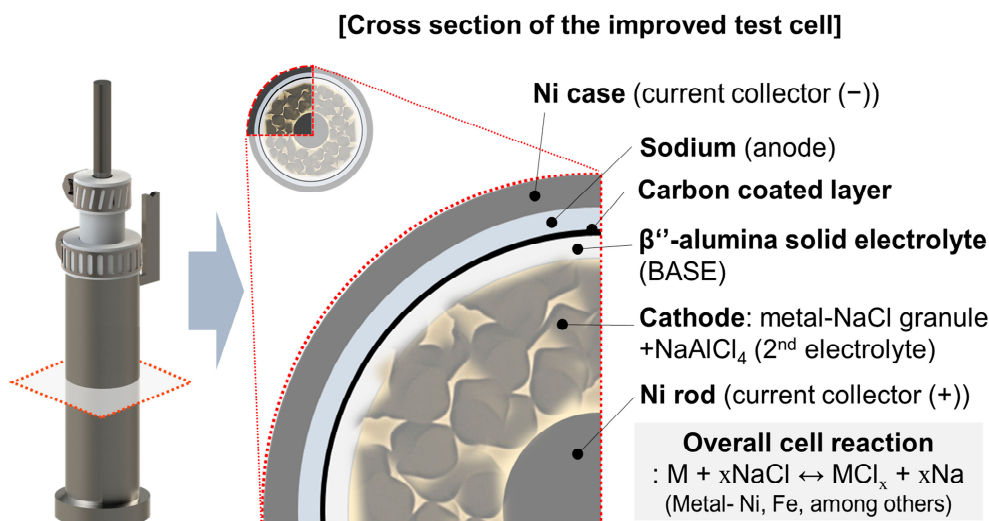


Figure 2. Schematic diagrams of tubular-type improved test cell structure and cross-section.

2.3. Electrochemical Test Setup

Previous test cells (PTC-1, 2, and 3) and improved test cells (ITC-1, 2, and 3) were tested inside the air-filled glove box that had sustained oxygen and moisture concentration of less than 1.0 ppm. The operation temperature was set up at 300 °C. These cells were cycled using VMP3 (Bio-Logic SAS, Seyssinet-pariset, Grenoble, France) between 2.4 V and 2.7 V, and the C-rates of previous test cells (PTC-1, 2, and 3) and improved test cells (ITC-1, 2 and 3) were set to C/24 and C/8, respectively. In the cases of PTC-4 and ITC-4 cells, a few cycles were started for stabilization before the constant capacity test. At the end of stabilization cycles, the charge process was started with a constant current method of 2.67 V, and then applied constant voltage method to the capacity of 200 mAh g⁻¹. In

contrast, the discharge process was conducted with only the constant current method set to capacity of 200 mAh g^{-1} and no cut-off voltage set-up. A limit for operation time was not set-up separately for PTC-4 and ITC-4 cells, however, ITC-4 cell was stopped due to the black-out after operating for approximately 7200 h.

3. Results and Discussion

We divided two test groups into previous test cells (PTC-1, 2, 3, and 4) and improved test cells (ITC-1, 2, 3, and 4). Condition details are noted in Table 1. Figure 3a,b show the cathode microstructure in the Na/NiCl_2 cell. In the case of Ni particles, the primary particle size is approximately under $1 \mu\text{m}$ and they form a chain structure that has a thickness of $2.5 \mu\text{m}$. NaCl particle size is $150\text{--}300 \mu\text{m}$, which is significantly larger than Ni. Therefore, Ni particles are located on the surface of the NaCl particle. Figure 3c,d indicate cathode microstructure in $\text{Na}/(\text{Ni}, \text{Fe})\text{Cl}_2$ cells. The difference from the Na/NiCl_2 cell is that Ni–Fe composite is used for the cathode metal. As seen in Figure 3c,d, Fe particles are located in the Ni network. The most important point in Ni–Fe composite is the selection of an appropriate particle size. Therefore, Fe particles larger than Ni particles are selected to obtain the effect of high connectivity as an electron path [24]. Figure 3e shows the XRD pattern of raw powders and cathode materials in the two test groups. The cathode materials are divided into charged state and discharged state. At the charged state in $\text{Na}(\text{Ni}, \text{Fe})\text{Cl}_2$ cell, the NiCl_2 peak indicates low intensity compared to the FeCl_2 peak, since most of Cl^- ions are almost reacted with Fe particles first. Ni particles are reacted with the residual Cl^- ions due to their higher electrochemical potential [24]. Therefore, it can be described that the Ni–Fe composite cathode microstructure is made as we intended.

Table 1. Initial charge capacity of previous test cells and improved test cells, and maximum charge capacity gap of each group.

Cell Name	Cell Type	Charge Capacity (% the 1st Cycle)	Maximum Capacity Gap (%)
PTC-1	Previous test cell (Ni foil type)	87.3	
PTC-2		62.8	37.2
PTC-3	Na/NiCl_2	100	
ITC-1	Improved test cell (Ni case type)	93.6	
ITC-2		100	9.5
ITC-3		90.5	

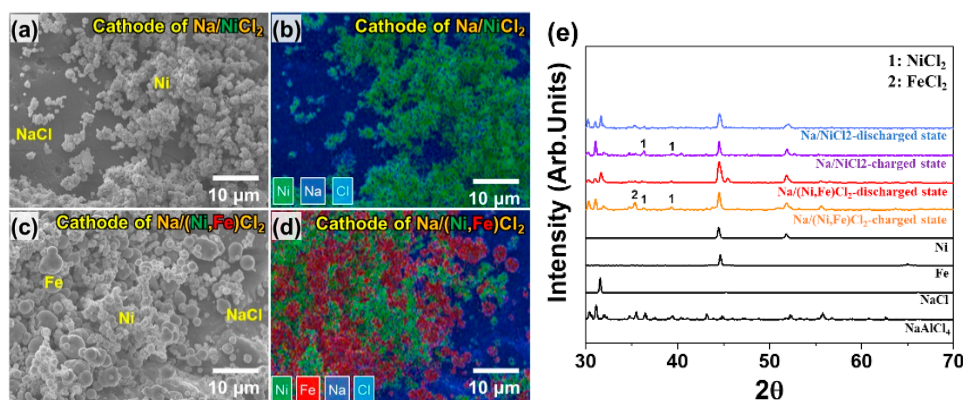


Figure 3. Cathode microstructure analysis. (a,b) SEM image and EDS mapping data of cathode material in Na/NiCl_2 cell (PTC-1 to 3 and ITC-1 to 3); (c,d) SEM image and EDS mapping data of cathode material in $\text{Na}/(\text{Ni}, \text{Fe})\text{Cl}_2$ cell. (PTC-4 and ITC-4); (e) X-ray diffraction (XRD) spectra of raw powder and cathode materials in two test groups.

Figure 4a,b show the voltage SOC profiles of the 1st cycle of previous test cells and improved test cells. The cells of PTC-1, 2, and 3 have the same composition of cathode materials as mentioned above, however, these cells have a large difference in the initial capacity of approximately 37.2%. This is caused by issues in the previous test cell structure. First, a Ni rod in the previous simple test cell was not fixed tightly except for the bottom side. The Ni rod could crush the elaborately designed cathode structure. Second, the Teflon cap was simply located on the top side. In this case, a seal of the cathode was not appropriate; therefore, a different amount of NaAlCl_4 was evaporated in each test. The quantity of evaporated NaAlCl_4 is different in each cell due to irregular closed levels. Hence, a large distribution of initial charge capacity was obtained despite the same cathode composition in the previous test cell group. By contrast, as shown in Figure 1, the structure of the improved test cell solves the problems of the previous test cell. A Teflon cap was tightly fixed by a hose clamp and perfectly closed the entrance of the cathode by using the characteristic that Teflon expands at an operation temperature of 300 °C. Moreover, a tightly fixed Teflon cap also held the Ni rod from wavering. Accordingly, the cells of ITC-1, 2, and 3 have a narrower capacity gap of 9.5% than that of previous test cells. As with the other group of previous test cells, all the improved test cells have the same cathode composition and test conditions. This narrower capacity gap means that the effect of test cell structure on the experimental result is reduced. Particularly, the electrochemical result of cathode microstructure analysis is more accurate by reducing the influence of other factors. PTC-1 to 3 and ITC-1 to 3 cells were tested under same electrochemical setup such as cut-off voltage and current. Nonetheless, the charging start voltage in the improved test cell is over 2.4 V, higher than the charging start voltage in the previous test cell. This high charging start voltage is due to the additional sodium metal in the anode Ni case. However, no problems have occurred in our research up to now because, for a section to reach approximately 2.60 V, which is the Ni charging voltage, is extremely minimal in terms of the whole charging reaction.

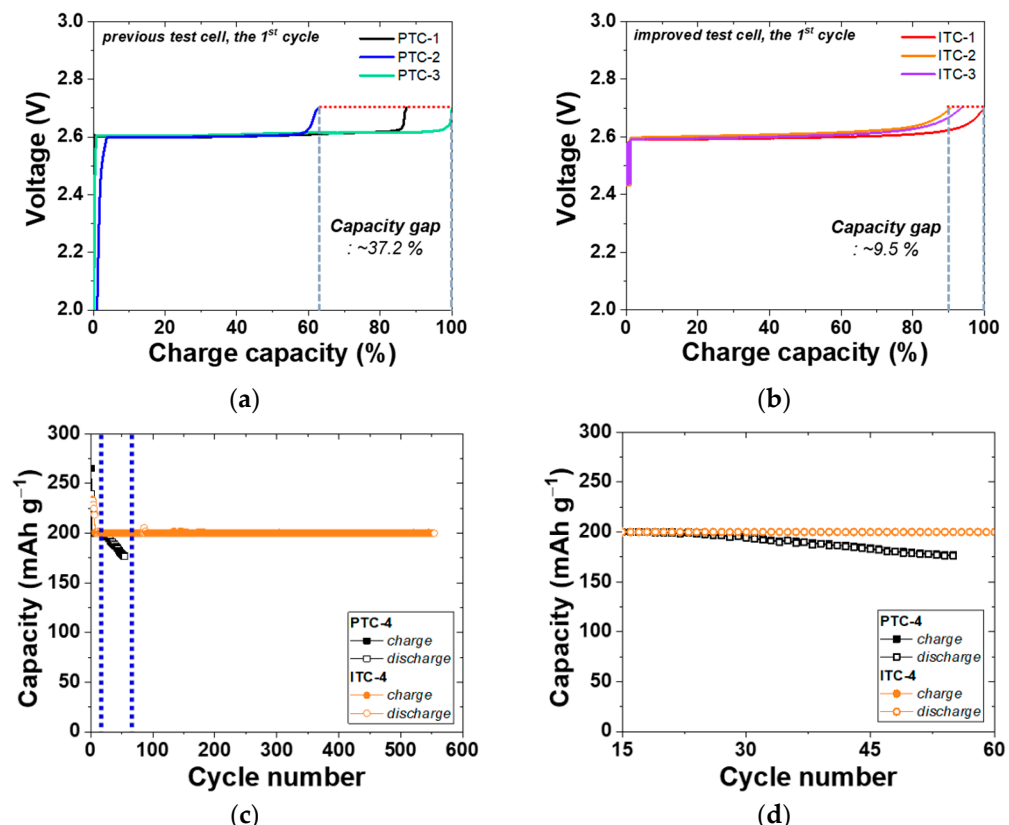


Figure 4. Cont.

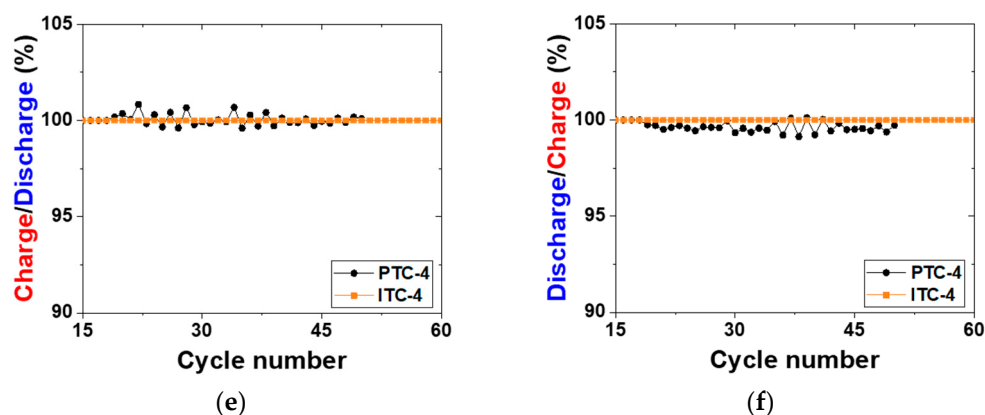


Figure 4. Electrochemical properties of test cells. (a,b) Voltage charge capacity profile of previous test cells and improved test cells for reproducibility analysis; (c,d) cycling performance of PTC-4 and ITC-4; (e) charge capacity ((n + 1)th cycle) divided by discharge capacity (nth cycle) profile; (f) discharge capacity (nth cycle) divided by charge capacity (nth cycle) profile.

To precisely compare the previous test cell and improved test cell, a cycle life test was conducted using two types of Na/(Ni, Fe)Cl₂ batteries, as indicated in Figure 4c and Table 2. In this test, a charge–discharge capacity was set up at 200 mAh g⁻¹, and the capacity was chosen because it is almost 80% of the 1st cycle charge capacity of the PTC-4 and ITC-4 cells. The charge process applied a constant current method to the charge capacity of 200 mAh g⁻¹ and a cut-off voltage of 2.67 V. If the charge capacity at the cut-off voltage of 2.67 V does not reach 200 mAh g⁻¹, the constant current method is switched to a constant voltage for attaining the charge capacity. In the discharge process, a test condition of a constant current method to the discharge capacity of 200 mAh g⁻¹ without cut-off voltage is set-up. Figure 4c shows the cycling performance of previous test cells and improved test cells. As mentioned above, the structural problems of previous test cells indicate a poor cycle life. The capacity of the PTC-4 cell decreases from the 23rd cycle and loses capacity maintenance. Capacity decrease can be caused by two points: an electron path disconnection in the cathode microstructure or sodium wicking. The disconnection problem can be detected from charge capacity divided by discharge capacity profile (charge/discharge), as shown in Figure 4e. The charge/discharge profile shows a ratio of (n + 1)th cycle charge capacity compared to the (n)th cycle discharge capacity. During a discharge process, NiCl₂ and FeCl₂ layers on the cathode metal particles are removed. However, when the cell has the poor microstructure of low-connectivity cathode, an electron path is also disconnected, along with the removal of metal chloride layers [25]. This disconnection occurs in isolated Ni or Fe particles that are unable to participate in the charge–discharge reaction. Namely, the charge/discharge profile indicates the stability of the cathode microstructure. A discharge/charge profile is also used to verify the test cell problem under the limited condition using our test cell in a sodium–metal chloride cell. The discharge/charge profile shows the ratio of the (n)th cycle discharge capacity compared with the (n)th cycle charge capacity. During a charge process in the sodium–metal chloride cell, NiCl₂ and FeCl₂ are formed on the Ni and Fe surface in the cathode, and sodium ions from NaCl migrate to the anode and settles. At this time, the problem of our previous test cell appears, whereby sodium metal is trapped on the BASE surface of the anode side, as shown in Figure 5c. The BASE surface of the anode side in our previous test cell is wrapped with an Al foil, and sodium wicking may occur due to the capillary effect in the vertical wrinkles of the Al foil. Trapped sodium metal on the BASE surface causes a loss in total capacity, because the residual Na metal cannot return to the cathode during the discharge reaction. In an ideal situation, there should be no residual sodium metal on the BASE surface and Al foil. (Figure 5a,b).

Table 2. Comparison of cycle life between PTC-4 and ITC-4.

Cell Name	Cell Type	Maintained Range of 200 mAh g ⁻¹
PTC-4	Na/(Ni, Fe)Cl ₂	Previous test cell To 23 cycles
ITC-4		Improved test cell To 554 cycles

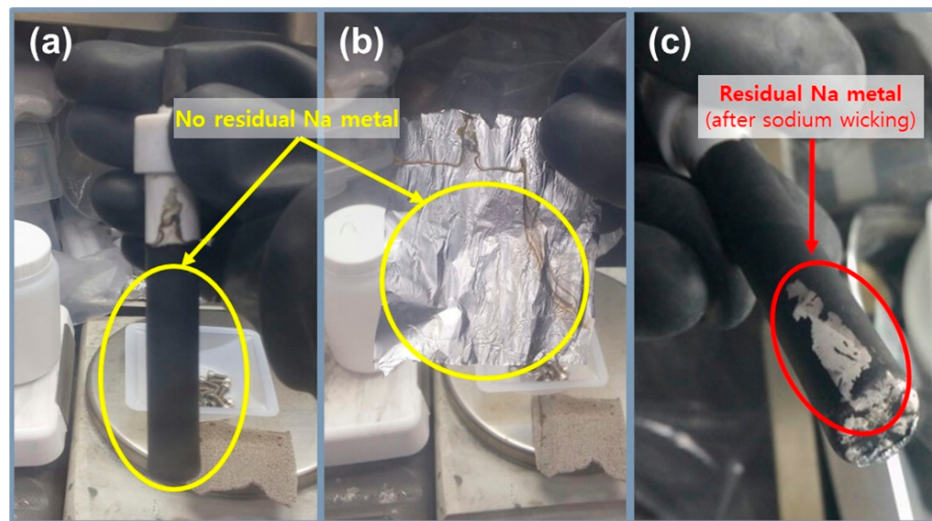


Figure 5. Photos of the previous test cell after cycling test, (a,b) no residual sodium metal on the BASE surface and Al foil; (c) the residual sodium metal (red circle) on the BASE surface after cycling test due to the capillary effect in the vertical wrinkles of the Al foil.

As seen in Figure 4e, charge/discharge profile of PTC-4 cell shows a value near 100% or over 100% in whole cycles. According to the above two cases, this charge/discharge profile of the PTC-4 cell suggests that the cathode microstructure of the PTC-4 cell is well-maintained during cycle life test. To be precise, the sodium wicking problem is expected to be the most important of the two causes of capacity decrease in the PTC-4 cell. However, the discharge/charge profile of the PTC-4 cell shows a value under 100% after the 17th cycle. This value means that the residual sodium is constantly trapped with each charge process. After the trapped sodium metal is clearly revealed, the charge–discharge capacity of the PTC-4 cell gradually decreases from the target capacity of 200 mAh g⁻¹. Although the PTC-4 cell has a stable cathode microstructure, the cycle life test of the PTC-4 cell fails due to the problems of the previous test cell structure. On the contrary, the ITC-4 cell has a stable cathode microstructure, and also none of the problems of the test cell structure. In the case of an improved test cell, an Ni case was applied with the sodium reservoir that is an important part for cathode microstructure analysis, due to the elimination of another failure case (trapped sodium) during a discharge reaction. As seen in Figure 6, despite the ITC-4 cell having a simple test cell structure, this cell was operated approximately 7200 h prior. This result shows that cycle life test is also possible using the improved simple test cell when the cathode microstructure is stable. By using the improved test cell in this study, it seems possible to actively develop cathode microstructure for tubular-type Na/MCl₂ batteries.

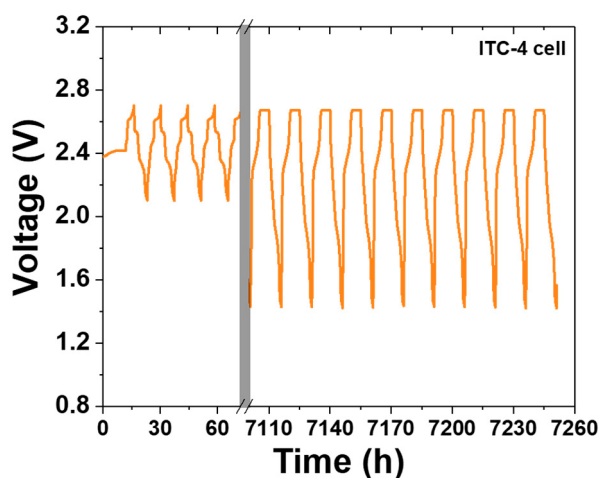


Figure 6. Voltage–time profile of ITC-4 cell for approximately 7200 h.

4. Conclusions

We designed an improved simple tubular test cell to analyze the cathode microstructure of sodium–metal chloride batteries by improving our previous test cell. The previous test cell has a low reproducibility and some problems with long duration cycle tests. The low reproducibility is occasioned by an imperfectly sealed structure and non-fixed Ni current collector that influences cathode materials directly. Moreover, residual sodium appears on the BASE surface by wicking to a narrow vertical wrinkle of Al foil. The residual sodium gradually increases with a repetitive charge–discharge process and causes a loss in total capacity. On the contrary, the improved test cell eliminates the leak and Ni rod (cathode current collector) wavering by using a Teflon cap and a hose clamp. Additionally, an Ni case is applied to the improved test cell, and then additional sodium metal is added in the Ni case to construct a sodium reservoir. By combining the improvements, factors that could affect the cell performance, except for cathode microstructure, are removed. The three improved cells obtain a capacity gap of 9.5%, and this value means that the reproducibility is improved compared to the capacity gap of the three previous test cells (37.2%). Furthermore, life cycle tests of the Na/(Ni, Fe)Cl₂ battery successfully finish after approximately 7200 h by using the improved test cell. Through the improvement of this tubular test cell, it is expected that sodium–metal chloride batteries can be studied more actively in a small and academic laboratory.

Author Contributions: Conceptualization, B.-M.A., C.-W.A. and J.-H.C.; formal analysis, B.-M.A. and C.-W.A.; investigation, B.-D.H. and J.-J.C.; methodology, Y.-D.K.; Writing—original draft preparation, B.-M.A.; Writing—review and editing, C.-W.A. and J.-H.C.; supervision, J.-H.C.; project administration, S.-K.L. and J.-H.C.; funding acquisition, S.-K.L. and J.-H.C. All authors have read and agreed to the published version of the manuscript.

Funding: This work was supported by the Korea Institute of Energy Technology Evaluation and Planning (KETEP) grant funded by the Korean government (MOTIE) (20172420108430) and by the Fundamental Research Program (PNK8110) of the Korea Institute of Materials Science.

Institutional Review Board Statement: Not applicable.

Informed Consent Statement: Not applicable.

Data Availability Statement: The data presented in this study are available from the corresponding authors upon reasonable request.

Conflicts of Interest: The authors declare no conflict of interest.

References

- Wang, Q.; Jiang, L.; Yu, Y.; Sun, J. Progress of enhancing the safety of lithium ion battery from the electrolyte aspect. *Nano Energy* **2019**, *55*, 93–114. [[CrossRef](#)]
- Wang, Y.; Gao, Q.; Wang, G.; Lu, P.; Zhao, M.; Bao, W. A review on research status and key technologies of battery thermal management and its enhanced safety. *Energy Res.* **2018**, *42*, 4008–4033. [[CrossRef](#)]
- Wang, Z.; Zhang, Y.; Jiang, H.; Wei, C.; An, Y.; Tan, L.; Xiong, S.; Feng, J. Free-standing $\text{Na}_2\text{C}_6\text{O}_6$ /MXene composite paper for high performance organic sodium-ion batteries. *Nano Res.* **2022**, *1–8*. [[CrossRef](#)]
- Ellis, B.L.; Nazar, L.F. Sodium and sodium-ion energy storage batteries. *Curr. Opin. Solid State Mater. Sci.* **2012**, *16*, 168–177. [[CrossRef](#)]
- Hueso, K.B.; Armand, M.; Rojo, T. High temperature sodium batteries: Status, challenges and future trends. *Energy Environ. Sci.* **2013**, *6*, 734–749. [[CrossRef](#)]
- Lu, X.; Xia, G.; Lemmon, J.; Yang, Z. Advanced materials for sodium-beta alumina batteries: Status, challenges and perspectives. *J. Power Sources* **2010**, *195*, 2431–2442. [[CrossRef](#)]
- O’Sullivan, T.M.; Bingham, C.M.; Clark, R.E. SPEEDAM 2006. In Proceedings of the International Symposium on Power Electronics, Electrical Drives, Automation and Motion, Taormina, Italy, 23–26 May 2006; p. 243.
- Javadi, T.; Petric, A. Thermodynamic Analysis of Reaction Products Observed in ZEBRA Cell Cathodes. *J. Electrochem. Soc.* **2011**, *158*, A700–A704. [[CrossRef](#)]
- Benato, R.; Cosciani, N.; Crugnola, G.; Sessa, S.D.; Lodi, G.; Parmeggiani, C.; Todeschini, M. Sodium nickel chloride battery technology for large-scale stationary storage in the high voltage network. *J. Power Sources* **2015**, *293*, 127–136. [[CrossRef](#)]
- Hosseinfar, M.; Petric, A. Effect of High Charge Rate on Cycle Life of ZEBRA. *J. Electrochem. Soc.* **2016**, *163*, A1226–A1231. [[CrossRef](#)]
- Veneri, O.; Capasso, C.; Patalano, S. Experimental study on the performance of a ZEBRA battery based propulsion system for urban commercial vehicles. *Appl. Energy* **2017**, *185*, 2005–2018. [[CrossRef](#)]
- Bracco, S.; Delfino, F.; Trucco, A.; Zin, S. Electrical storage systems based on Sodium/Nickel chloride batteries: A mathematical model for the cell electrical parameter evaluation validated on a real smart microgrid application. *J. Power Sources* **2018**, *399*, 372–382. [[CrossRef](#)]
- Li, G.; Lu, X.; Kim, J.Y.; Lemmon, J.P.; Sprenkle, V.L. Cell degradation of a $\text{Na}-\text{NiCl}_2$ (ZEBRA) battery. *J. Mater. Chem. A* **2013**, *1*, 14935–14942. [[CrossRef](#)]
- Kim, S.M.; Lee, S.-M.; Jung, K.; Park, Y.-C.; Cho, N.-U.; Choi, J.-H.; Kim, H.-S. Influence of Carbon Coating on Beta-Alumina Membrane for Sodium-Nickel Chloride Battery. *Kor. Chem. Soc.* **2015**, *36*, 2869–2874. [[CrossRef](#)]
- Kim, J.; Jo, S.H.; Bhavaraju, S.; Eccleston, A.; Kang, S.O. Low temperature performance of sodium-nickel chloride batteries with NaSICON solid electrolyte. *J. Electroanal. Chem.* **2015**, *759*, 201–206. [[CrossRef](#)]
- Kim, S.-M.; Lee, S.-M.; Jung, K.; Park, Y.-C.; Cho, N.-U.; Kim, H.-S. Feasibility Study of a Planar-type Sodium—Nickel Chloride Battery. *Kor. Chem. Soc.* **2016**, *37*, 695–699. [[CrossRef](#)]
- Lu, X.; Chang, H.J.; Bonnett, J.F.; Canfield, N.L.; Jung, K.; Sprenkle, V.L.; Li, G. Effect of cathode thickness on the performance of planar $\text{Na}-\text{NiCl}_2$ battery. *J. Power Sources* **2017**, *365*, 456–462. [[CrossRef](#)]
- Chang, H.J.; Canfield, N.L.; Jung, K.; Sprenkle, V.L.; Li, G. Advanced $\text{Na}-\text{NiCl}_2$ Battery Using Nickel-Coated Graphite with Core—Shell Microarchitecture. *ACS Appl. Mater. Interfaces* **2017**, *9*, 11609–11614. [[CrossRef](#)]
- Chang, H.J.; Lu, X.; Bonnett, J.F.; Canfield, N.L.; Son, S.; Park, Y.-C.; Jung, K.; Sprenkle, V.L.; Li, G. Development of intermediate temperature sodium nickel chloride rechargeable batteries using conventional polymer sealing technologies. *J. Power Sources* **2017**, *348*, 150–157. [[CrossRef](#)]
- Li, G.; Lu, X.; Kim, J.Y.; Meinhardt, K.D.; Chang, H.J.; Canfield, N.L.; Sprenkle, V.L. Advanced intermediate temperature sodium-nickel chloride batteries with ultra-high energy density. *Nat. Commun.* **2016**, *7*, 10683. [[CrossRef](#)]
- Li, Y.; Wu, X.; Wang, J.; Gao, X.; Hu, Y.; Wen, Z. Ni-less cathode with 3D free-standing conductive network for planar $\text{Na}-\text{NiCl}_2$ batteries. *Chem. Eng. J.* **2020**, *387*, 124059. [[CrossRef](#)]
- Li, Y.; Shi, L.; Gao, X.; Wang, J.; Hu, Y.; Wu, X.; Wen, Z. Constructing a charged-state $\text{Na}-\text{NiCl}_2$ battery with NiCl_2 /graphene aerogel composite as cathode. *Chem. Eng. J.* **2021**, *421*, 127853. [[CrossRef](#)]
- Li, G.; Lu, X.; Kim, J.Y.; Viswanathan, V.V.; Meinhardt, K.D.; Engelhard, M.H.; Sprenkle, V.L. An Advanced $\text{Na}-\text{FeCl}_2$ ZEBRA Battery for Stationary Energy Storage Application. *Adv. Energy Mater.* **2015**, *5*, 1500357. [[CrossRef](#)]
- Ahn, B.-M.; Ahn, C.-W.; Hahn, B.-D.; Choi, J.-J.; Kim, Y.-D.; Lim, S.-K.; Jung, K.; Park, Y.-C.; Choi, J.-H. Easy approach to realize low cost and high cell capacity in sodium nickel-iron chloride battery. *Compos. Part B* **2019**, *168*, 442–447. [[CrossRef](#)]
- Ahn, B.-M.; Ahn, C.-W.; Hahn, B.-D.; Choi, J.-J.; Kim, Y.-D.; Lim, S.-K.; Choi, J.-H. Effect of Cathode Microstructure on Electrochemical Properties of Sodium Nickel-Iron Chloride Batteries. *Materials* **2021**, *14*, 5605. [[CrossRef](#)]